

Ferrite optimization for a three-phase wireless power transfer system for electric vehicles

Shuang Nie, Mehanathan Pathmanathan, Peter W. Lehn

Department of Electrical Computer Engineering, Faculty of Applied Science and Engineering

University of Toronto, Toronto, Canada

shuang.nie@mail.utoronto.ca

Acknowledgement

This work was supported by the Natural Sciences and Engineering Research Council of Canada (NSERC) under Grant CRDPJ 513206-17.

Keywords

«Wireless power transmission», «Electric vehicle», «Charging Infrastructure for EV's», «Passive component», «Modelling»

Abstract

This paper proposes a new design for placement of the ferrite in high power three-phase EV wireless power transfer systems. The paper analyzes ferrite designs with variations in orientation, size and position. The proposed design reduces ferrite usage, lowers required excitation voltage and improves DC-DC efficiency.

Introduction

Over the last decade, electric vehicles (EVs) have become a viable option for transportation electrification where pollution from transportation emission can be massively reduced. Developing EV charging facilities is critical for resolving the drive range concern which is the largest barrier for EV market expansion. Wireless power transfer (WPT) is a contactless charging technique for EV which can minimize the electrocution risk and ensure user safety during the charging process.

Three-phase coil designs in wireless power transfer have been investigated in recent years as alternative to conventional wireless power transfer prototypes such as the circular pad (CP), bipolar pad DD pad and DDQ pad [1]. Pathmanathan et al. [2] proposed a method of designing a three-phase WPT transmitter analogous to the stator windings of a three-phase, two-pole electrical machine. Pries et al. [3] developed a three-phase inductive WPT systems with bipolar phase windings to improve power density and specific power of wireless charging systems for high-power applications.

Most existing commercial WPT three-phase pads for stationary charging use large quantities of the magnetic material ferrite [3][4]. Ferrite can significantly improve the magnetic performance and power transfer, but has the disadvantage of being brittle and can increase the system cost [5]. Mohammad et al. proposed a design and optimization method of ferrite cores for a single coil to single coil wireless charging system to improve its misalignment tolerance and minimize the core loss [6]. This paper proposes a ferrite optimization design of the three-phase stationary wireless charging system. The proposed design achieved higher DC-DC efficiency at receiver misaligned case after reducing ferrite by around 40% and lowered the required driving DC bus voltage by 62% at max in the experimental measurement.

Ferrite optimization for a three-phase transmitter

Three-phase transmitter modeling

The coil structure for a typical three-phase wireless power transfer system is presented in Fig. 1. The power is delivered by injecting AC currents into three transmitter coils (named as coil A, coil B and coil C) to generate a compound magnetic flux waveform at the receiver coil. The receiver coil picks up the magnetic flux and the resulting induced voltage can provide power to a resistor or battery load. The SAE J2954 standard states that the leakage flux outside the charging zone has to be less than 27 uT at 100 kHz to ensure user safety. As a result, shielding material such as ferrite and aluminum are added on both transmitter and receiver sides to reshape the magnetic field into an enclosed loop contained inside the charging zone.

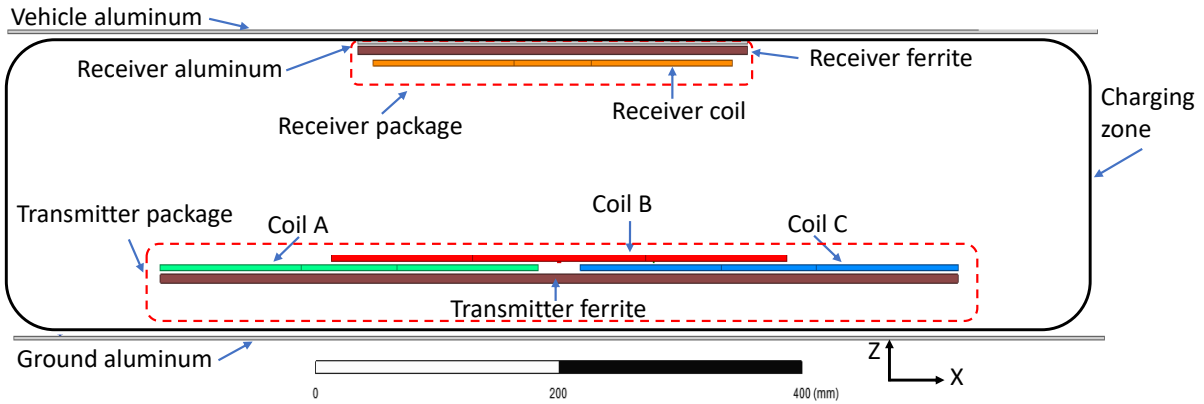


Fig. 1: Three-phase coil structure with ferrite and aluminum

The impact of ferrite on the system appears as variation in the inductance matrix. For a three-phase charging system, a 4×4 inductance matrix is constructed: (all value are in rms):

$$\begin{bmatrix} V_a \\ V_b \\ V_c \\ 0 \end{bmatrix} = \begin{bmatrix} Z_a & j\omega M_{ab} & j\omega M_{ac} & j\omega M_{ar} \\ j\omega M_{ba} & Z_b & j\omega M_{bc} & j\omega M_{br} \\ j\omega M_{ca} & j\omega M_{cb} & Z_c & j\omega M_{cr} \\ j\omega M_{ra} & j\omega M_{rb} & j\omega M_{rc} & Z_r + R_{L,eq} \end{bmatrix} \begin{bmatrix} I_a \\ I_b \\ I_c \\ I_r \end{bmatrix}, \quad Z_n = j\omega L_n - \frac{j}{\omega C_n} + R_n \quad (1)$$

where R_n is the effective coil total resistance, $R_{L,eq}$ is the equivalent resistance of load, L_n is the self-inductance, M_{nm} is the mutual inductance, ω is the angular frequency of the excitation current, and C_n is the series compensation capacitance. The effective coil total resistance of each transmitter phase R_n is a sum of litz wire AC resistance at ω , additional effective resistance caused by aluminum sheet eddy current loss and additional effective resistance caused by ferrite core loss. For coil n , the coil is self-compensated where $C_n = \frac{1}{\omega^2 L_n}$. The matrix is symmetric with $M_{nm} = M_{mn}$.

Table I: Characteristics of each entries of the inductance matrix

Description	Parameter	Main system effect	Correlation
T-T mutual inductance	M_{ab}, M_{ac}, M_{bc}	excitation voltage	positive
T-R mutual inductance	M_{ar}, M_{br}, M_{cr}	system coil efficiency	positive
Self inductance	L_a, L_b, L_c	capacitor voltage stress	positive
Effective coil total resistance	R_a, R_b, R_c	system coil efficiency	negative

T-T: transmitter-transmitter, T-R: transmitter-receiver

Based on past WPT research, the characteristic of each matrix entry is summarized in the Table I. For example, from row 1, a positive correlation indicates that higher transmitter-transmitter mutual inductance requires a high excitation voltage, thus a high DC bus voltage. All the parameters in the Table I can be affected by the placement of ferrite and aluminum. As shown in the Fig. 1, the size and position

of the vehicle aluminum sheet and ground aluminum sheet are fixed to contain the entire charging zone. The receiver ferrite is commonly the same size as the receiver coil with a small ferrite-coil distance. In this paper, the transmitter ferrite is optimized to determine its orientation, size and location.

Transmitter-transmitter mutual inductances and DC bus voltage

For a practical three-phase wireless power transfer application, a low excitation and DC bus voltage is required to ensure the interoperability of the three-phase wireless system and available DC power supply equipment. The DC bus voltage is mainly impacted by the transmitter-transmitter mutual inductances. By reformatting each row of (1) and substituting $C_n = \frac{1}{\omega^2 L_n}$, the transmitter voltage for each phase can be derived as:

$$\mathbf{V}_a = \mathbf{I}_a R_a + j\omega(M_{ar}\mathbf{I}_r + M_{ab}\mathbf{I}_b + M_{ac}\mathbf{I}_c) \quad (2)$$

$$\mathbf{V}_b = \mathbf{I}_b R_b + j\omega(M_{br}\mathbf{I}_r + M_{ba}\mathbf{I}_a + M_{bc}\mathbf{I}_c) \quad (3)$$

$$\mathbf{V}_c = \mathbf{I}_c R_c + j\omega(M_{cr}\mathbf{I}_r + M_{ca}\mathbf{I}_a + M_{cb}\mathbf{I}_b) \quad (4)$$

where,

$$\mathbf{V}_a = V_{a,rms}/\theta_a, \mathbf{V}_b = V_{b,rms}/\theta_b, \mathbf{V}_c = V_{c,rms}/\theta_c \quad (5)$$

$$V_{dc} = \max\{V_{a,rms}, V_{b,rms}, V_{c,rms}\}\pi/\sqrt{2} \quad (6)$$

From (2)-(4), the reactive voltage of each phase is determined by the product of transmitter phase current and transmitter-transmitter mutual inductance. As transmitter-transmitter mutual inductance increases, the magnitude of each phase voltage increases. The DC bus voltage required for exciting the three-phase wireless system is determined by the maximum phase voltage among all three phases as shown in (6). Overall, large transmitter-transmitter mutual inductances lead to high phase voltages thus a high DC bus voltage.

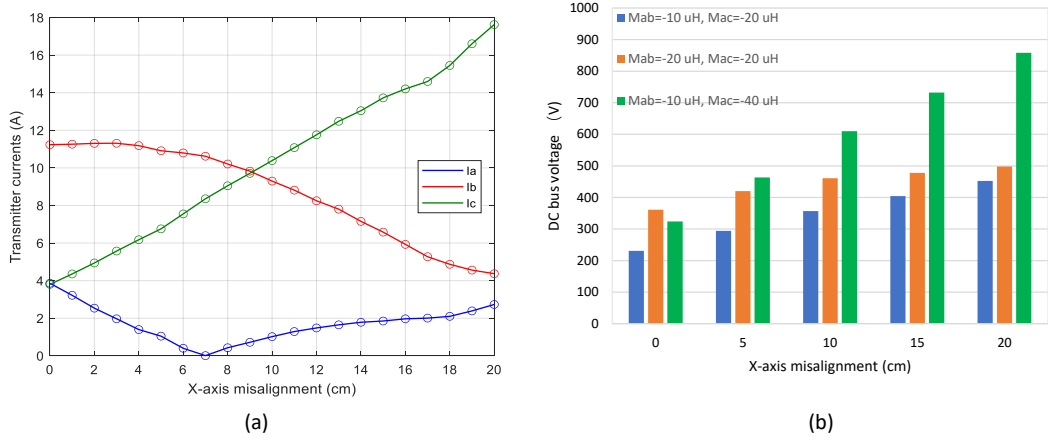


Fig. 2: a) Three-phase system transmitter current magnitude b) required DC bus voltage for different transmitter-transmitter mutual inductances under receiver X-axis misalignment

Fig. 2 (a) presents the transmitter current distribution for a typical three-phase wireless system under different receiver X-axis misalignment [7]. The transmitter current distribution is optimized to achieve the highest coil efficiency for different receiver X-axis misalignment. Fig. 2 (b) displays the required DC bus voltage for a 1 kW three-phase wireless power transfer under different receiver X-axis misalignment. The DC bus voltages are calculated based on the transmitter currents in Fig. 2 (a) and different combinations of transmitter-transmitter mutual inductances M_{ab} , M_{bc} and M_{ac} . From Fig. 1, M_{ab} equals M_{bc} due to the symmetry of three-phase coil structure. $M_{ab} = -10 \mu H$, $M_{ac} = -20 \mu H$ is selected as the base case since it is difficult to construct a perfectly decoupled transmitter pad in practice. The magnitude of M_{ab} is typically lower than the magnitude of M_{ac} since the overlapping distance among adjacent coils can be

adjusted more easily whereas the side coil A,C distance is limited by the total transmitter pad size. Fig. 2 (b) presents how M_{ab} or M_{ac} impacts the DC bus voltage. By comparing the orange bar with the blue bar, it is seen that M_{ab} has a larger impact on the DC bus voltage as when the receiver is perfectly aligned. This is apparent as the DC bus voltage for the orange bar is 56% greater than the blue bar at X=0 cm but only 10% greater at X=20 cm. By comparing the green bar with the blue bar, it is clear that M_{ac} has a larger impact on the DC bus voltage when the receiver is misaligned. This can be seen from the DC bus voltage of the green bar being 90% higher than the blue bar at X=20 cm but only 40% higher at X=0 cm. It is also important to highlight that the DC bus voltage increases as receiver misalignment increases for all transmitter-transmitter mutual inductance values. The height of the blue bar is almost doubled from X=0 cm to X=20 cm receiver misalignments. Thus, in order to reduce the required DC bus voltage, both M_{ab} and M_{ac} need to be minimized by the ferrite placement optimization. In particular, M_{ac} needs to be minimized to reduce the maximum DC bus voltage which occurs at receiver extreme misalignment.

Ferrite orientation

Many WPT designs place a large ferrite pad beneath the transmitter pad to reduce the eddy current loss in the aluminum shield and increase the transmitter-receiver mutual inductances for efficiency improvement. However, a larger ferrite pad can generate high core loss in the ferrite itself due to the eddy current conducting along the internal loop. A typical method to reduce the core loss is to replace one integral ferrite pad with many small ferrite blocks. Air gap are fixed between each ferrite block which prevents the eddy current flowing and reduces the core loss.

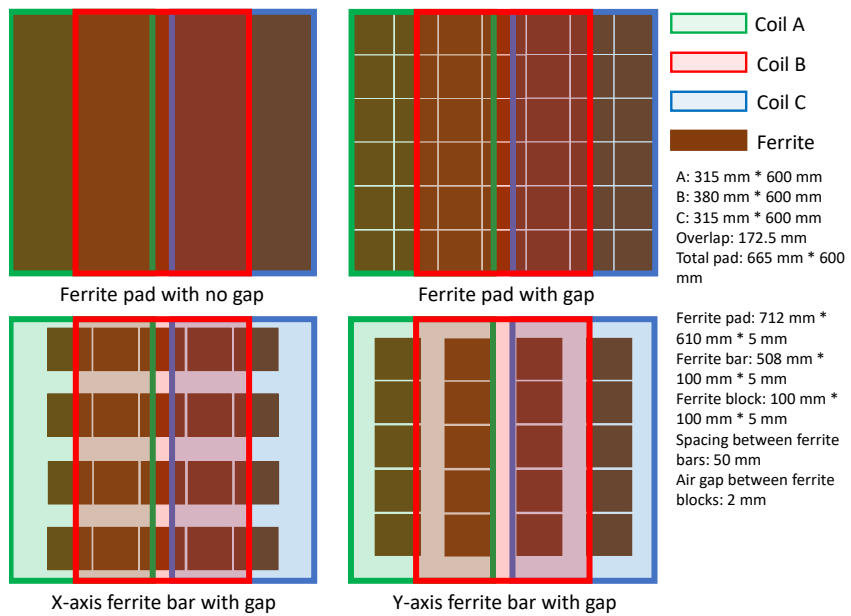


Fig. 3: Transmitter ferrite placement orientation

To optimize the ferrite placement, the first step is to determine the ferrite orientation. Fig. 3 shows the view from the top of the three-phase transmitter pad where three types of ferrite placements are compared. The dimensions of each coil and different ferrite placements are given. The X-axis direction is defined in Fig. 1 which is the door-door direction of a vehicle while the Y-axis is the in vehicle driving direction. Typically the X-axis misalignment of the receiver is a challenge as the Y-axis misalignment can be resolved by driving the vehicle forward and backward. This paper adopts PC95 power ferrite from TDK which has a high saturation flux density 0.5 T.

In Table II, the effective coil total resistance at 85 kHz for each orientation with and without air gap is simulated through ANSYS Maxwell loss models. By comparing the top two rows of Table II, it is obvious that the air gap can reduce the core loss significantly. The effective coil total resistance values of the three orientations are similar since the core loss difference is minimized by the air gap.

Table II: Simulated effective coil total resistance value of different orientation

Orientation	$R_a(m\Omega)$	$R_b(m\Omega)$	$R_c(m\Omega)$
Ferrite pad (no gap)	604	950	604
Ferrite pad (with gap)	233	370	233
X-axis ferrite bar (with gap)	214	374	214
Y-axis ferrite bar (with gap)	212	344	212

The inductance matrices are derived from ANSYS Maxwell for all four types of orientations.

$$\mathbf{L}_{pad,no\ gap} = \begin{bmatrix} 478.1 & -6.9 & -62.3 & 3.5 \\ -6.9 & 539.2 & -8.1 & 26.9 \\ -62.3 & -8.1 & 472.5 & 3.5 \\ 3.5 & 26.9 & 3.5 & 183.2 \end{bmatrix} \mu H \quad \mathbf{L}_{pad,gap} = \begin{bmatrix} 425.4 & -7.2 & -37.2 & 3.1 \\ -7.2 & 475.8 & -7.5 & 23.5 \\ -37.2 & -7.5 & 422.8 & 3.1 \\ 3.1 & 23.5 & 3.1 & 182.8 \end{bmatrix} \mu H$$

$$\mathbf{L}_{Xbar,gap} = \begin{bmatrix} 329.6 & -33.5 & -46.5 & 0.4 \\ -33.5 & 421.0 & -33.1 & 20.7 \\ -46.5 & -33.1 & 328.2 & 0.4 \\ 0.4 & 20.7 & 0.4 & 185.0 \end{bmatrix} \mu H \quad \mathbf{L}_{Ybar,gap} = \begin{bmatrix} 297.8 & -23.1 & -19.8 & 1.6 \\ -23.1 & 310.0 & -23.1 & 16.5 \\ -19.8 & -23.1 & 297.8 & 1.6 \\ 1.6 & 16.5 & 1.6 & 184 \end{bmatrix} \mu H$$

By comparing the inductance matrices, it is obvious that the Y-axis ferrite bar with gap case has the advantages of reducing the transmitter-transmitter mutual inductance M_{ac} . As discussed in the previous section, the low transmitter-transmitter mutual inductance can reduce the required input DC voltage. However, the Y-axis ferrite bar with gap case decreases the transmitter-receiver mutual inductance compared with the ferrite pad with gap case. The transmitter-transmitter mutual inductance between adjacent coils, M_{ab}, M_{bc} increase due to the two center ferrite bars placed at the intersection region of the adjacent coils as shown in Fig. 3. Both the transmitter-receiver mutual inductance and the adjacent transmitter-transmitter mutual inductance can be improved by further optimization of the Y-axis ferrite bar size and location.

Ferrite orientation experimental measurement

Fig. 4 shows the three-phase transmitter pad constructed using NELD 1100/40SNSN type 2 litz wire (AWG 10) from New England Wire Technologies and the three types of ferrite orientation with gap. A single continuous piece of ferrite with sufficiently large dimensions to construct the ungapped ferrite pad is not available (as the PC95 power ferrite was only available in maximum dimensions of 100 mm * 100 mm * 5 mm). The later analysis in this manuscript is based on ferrite placements all with air gap considered. Table III displays the measured effective coil total resistances for the three types of orientation. The measured resistance values have small discrepancy with the simulated resistance values in the previous section.

Table III: Measured effective coil total resistance value of different orientation

Orientation	$R_a(m\Omega)$	$R_b(m\Omega)$	$R_c(m\Omega)$
Ferrite pad (with gap)	286	440	280
X-axis ferrite bar (with gap)	257	433	255
Y-axis ferrite bar (with gap)	273	419	263

The inductance matrices for all three types of orientation are measured by the Hioki impedance analyzer IM3570 (matrices from left to right, ferrite pad with gap, X-axis ferrite bar with gap, Y-axis ferrite bar with gap. The unit is in μH).

$$\begin{bmatrix} 436.4 & -5.4 & -41.3 & 3.5 \\ -5.4 & 492.1 & -6.1 & 24.2 \\ -41.3 & -6.1 & 435.3 & 3.3 \\ 3.5 & 24.2 & 3.3 & 171.4 \end{bmatrix} \begin{bmatrix} 336.1 & -40.2 & -53.7 & 1.2 \\ -40.2 & 430.3 & -36.8 & 21.0 \\ -53.7 & -36.8 & 335.9 & 1.1 \\ 1.2 & 22.1 & 1.1 & 170.8 \end{bmatrix} \begin{bmatrix} 297.2 & -19.8 & -20.3 & 1.9 \\ -19.8 & 318.9 & -26.0 & 17.1 \\ -20.3 & -26.0 & 299.0 & 1.7 \\ 1.9 & 17.1 & 1.7 & 171.2 \end{bmatrix}$$

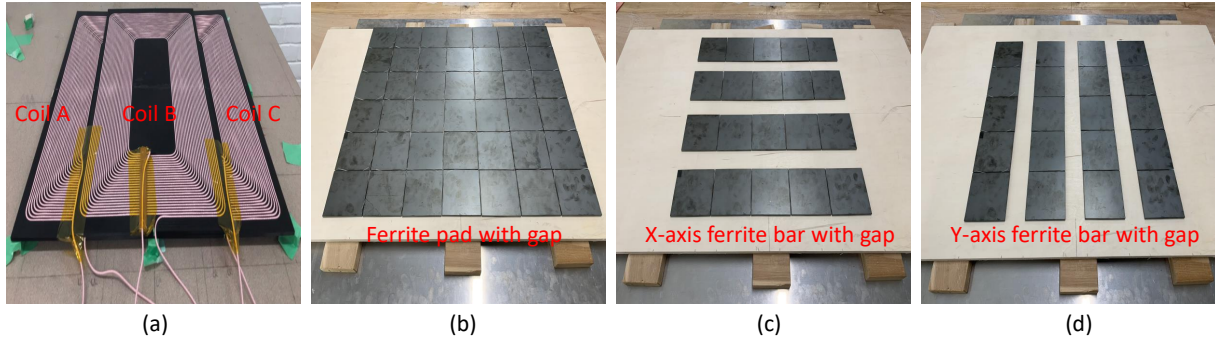


Fig. 4: (a) Three-phase transmitter coils, (b) Ferrite pad with gap, (c) X-axis ferrite bar with gap, (d) Y-axis ferrite bar with gap

The measured inductance matrices have small discrepancy with the simulated inductance matrices in the previous section. Based on the measured inductance matrices , the Y-axis ferrite bar is selected as the ferrite orientation due to its ability to decrease the transmitter-transmitter mutual inductance M_{ac} .

Ferrite size and position

With the ferrite bar orientation determined to be along the Y-axis, the ferrite size and position are optimized to increase the transmitter-receiver mutual inductance and further reduce the transmitter-transmitter mutual inductances. From Fig. 2 (b), it is known that the maximum DC bus voltage required occurs at receiver extreme misalignment. Therefore, the ferrite optimization process starts by assuming receiver centered above the transmitter, and ends with receiver at extreme misalignment to ensure that the final optimized DC bus voltage does not exceed the power electronics limit. To simplify the optimization process, one ferrite bar is chosen to enhance the coupling of each coil. A 25 mm (width) * 508 mm (length) * 5 mm (thickness) thin bar is placed beneath the center of each coil, as per Fig. 5 (a). The thin bar adopt five 25 mm * 100 mm * 5 mm ferrite blocks with a 2 mm air gap between each two blocks. The ferrite width and the ferrite-coil Z distance are selected as design variables since these two variables have highest impact on the transmitter-transmitter mutual inductances M_{ab} and M_{ac} .

Six critical parameters M_{ac} , M_{ab} , V_{dc} , R_b , M_{br} and η_{coil} are plotted in Fig. 5 (b), (c), (d), (e), (f) and (g). For each combination of ferrite width and ferrite-coil Z distance, the inductance matrix and effective coil total resistances of the three-phase coil system can be derived from ANSYS Maxwell simulation. Based on the inductance matrix and effective coil total resistances, the current distribution of each phase can be obtained through the optimal excitation method in [7]. The DC bus voltage V_{dc} can be derived from the current distribution and the transmitter-transmitter mutual inductances following (2)-(6). The red plane in Fig. 5 (d) indicates the boundary of V_{dc} for which the points below the plane are considered as preferred solution range. The highest DC bus voltage preferred due to the power electronic limit is 400 V. From Fig. 2 (b), the ratio between the DC bus voltage at receiver extreme misalignment ($X=20$ cm) and the DC bus voltage at receiver perfect alignment ($X=0$ cm) varies from 1.4 to 2.6. The median 2 is selected to be the ratio between DC bus voltages at $X=20$ cm and $X=0$ cm. Therefore, to ensure that the DC bus voltage is below 400 V at $X=20$ cm, the DC bus voltage limit (red plane in (d)) for the $X=0$ cm case is set as $400/2=200$ V.

Based on the derived current distribution and the simulated effective coil total resistances, the coil efficiency can be calculated as:

$$\eta_{coil} = \frac{P_{out}}{P_{out} + (I_a^2 * R_a + I_b^2 * R_b + I_c^2 * R_c + I_r^2 * R_r)} \quad (7)$$

Observing Fig.5 (d) and Fig.5 (g) together, the optimized ferrite width and ferrite-coil Z distance for the receiver centered case are determined from the point (red star in (g)) with the highest coil efficiency within the feasible range determined from figure (d). The ferrite width is selected to be 100 mm while the ferrite-coil Z distance is selected to be 10 mm.

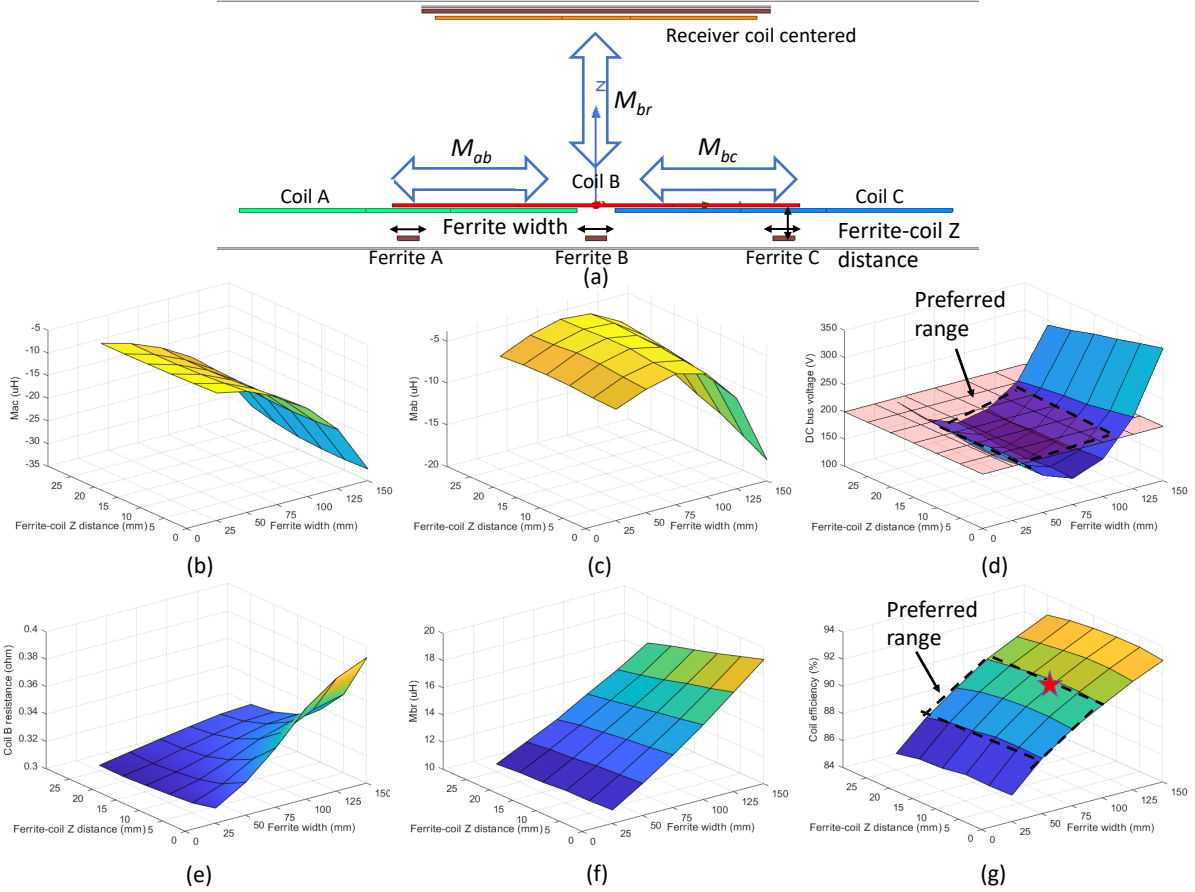


Fig. 5: (a) Three-phase coil structure as receiver coil centered, (b) M_{ac} , (c) M_{ab} , (d) V_{dc} , (e) R_b , (f) M_{br} , (g) η_{coil}

From the above design, the optimal ferrite width for all ferrites (A, B and C) and ferrite-coil Z distance are determined under receiver perfect alignment case. For the receiver extreme misalignment case ($X=20$ cm), the three-phase system performs similar to the single coil system where the side coil (A or C) is conducting the highest current as shown in Fig. 2 (a). Therefore, ferrite A and C ferrite can be re-optimized to enhance the performance of side coil when receiver misaligned as shown in Fig.6 (a). Width of ferrite A,C and ferrite-ferrite center distances are selected as design variables. To ensure symmetry of the three-phase coil system, the width of ferrite A is equal to the width of ferrite C and the ferrite A-B center distance is equal to the ferrite B-C center distance. Based on the previous optimization result, width of ferrite B remains constant as 100 mm. Ferrite-coil Z distance for all ferrites remain constant as 10 mm.

Side ferrite A and C are optimized by plotting M_{ac} , M_{ab} , V_{dc} , R_a , M_{ar} and η_{coil} with respect to ferrite A,C width and ferrite A-B(B-C) center distance in Fig. 6. The red plane in Fig. 6 (d) indicates the boundary of V_{dc} for which the points below the plane are considered as preferred solution range. As mentioned above, the maximum DC bus voltage due to power electronics limit is 400 V. Therefore, the red plane is set as 400 V to filter out the combinations of ferrite A,C width and ferrite A-B(B-C) center distance which results in a high DC bus voltage. Fig. 6 (g) presents the coil efficiency at receiver misaligned case derived from (7). From the feasible range determined in Fig. 6 (d), the same range can be plotted in Fig. 6 (g). The red star with the highest coil efficiency in the preferred range is selected to be the optimal point.

The final ferrite width are 200 mm for ferrite A, 100 mm for ferrite B and 200 mm for ferrite C. The final ferrite-ferrite center distance is 200 mm for A-B and 200 mm for B-C. The final ferrite-coil Z distance is 10 mm for all three ferrite bars.

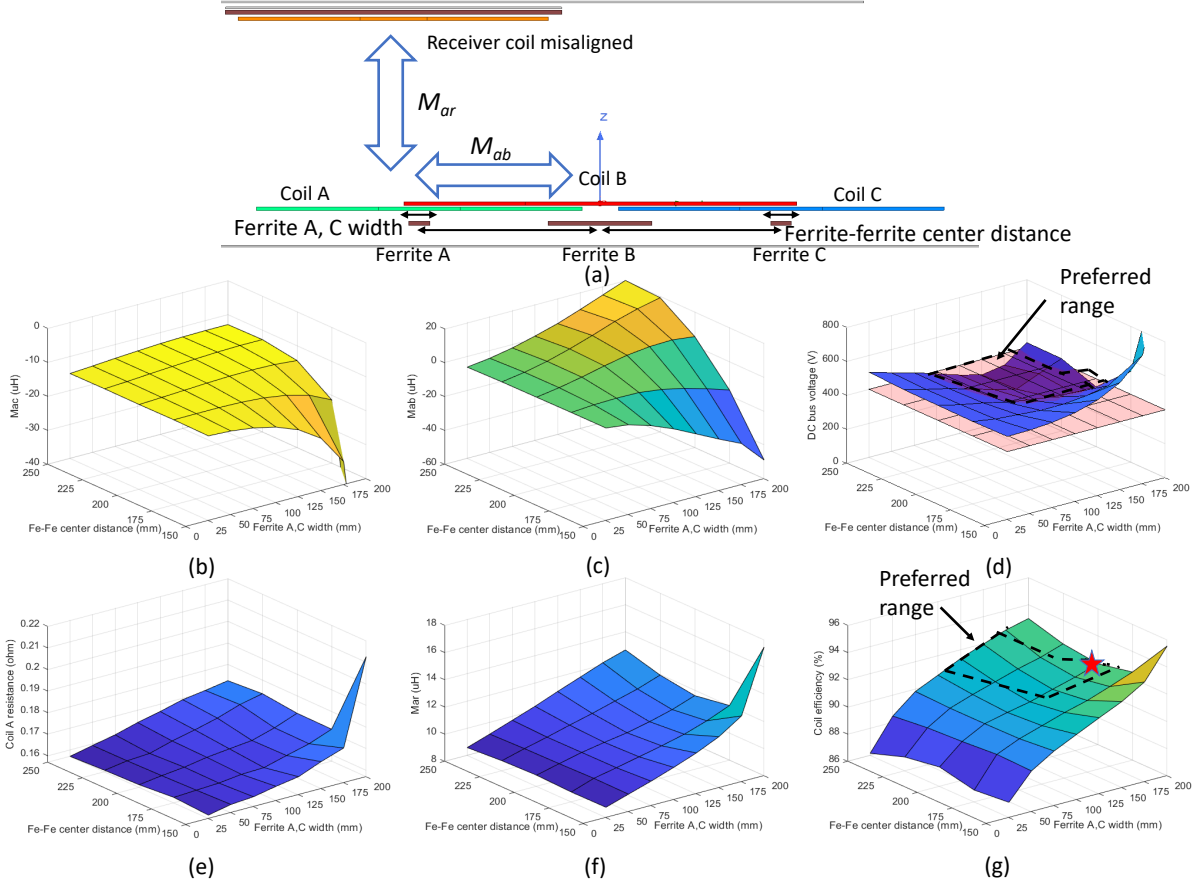


Fig. 6: (a) Three-phase coil structure as receiver coil misaligned to X=20 cm, (b) M_{ac} , (c) M_{ab} , (d) V_{dc} , (e) R_a , (f) M_{ar} , (g) η_{coil}

Ferrite size and position experimental measurement

Five different pairs of ferrite width and ferrite-coil Z distance are selected to validate the simulation result shown in Fig. 5. Table IV displays the measured inductance matrix values and effective coil total resistances for the selected pairs. The comparison among pairs P1, P2 and P3 indicates how the inductance matrix values and effective coil total resistances vary with ferrite width when the ferrite-coil Z distance remain constant. The comparison among P2, P4 and P5 indicates how the inductance matrix values and effective coil total resistances vary with the ferrite-coil Z distance when the ferrite width remain constant. The measured inductance and resistance values matches the simulated result in Fig. 5 within an acceptable error. The last two columns of Table IV display the estimated DC bus voltage and coil efficiency derived from the measured inductance matrix and effective coil total resistances in Table IV. Among all the pairs P1-P5, P3 is disqualified due to the large V_{dc} values which exceeded the preferred solution range $V_{dc} \leq 200$ V. By comparing remaining pairs, P5 is selected to be the optimal pair since it has the highest coil efficiency. Therefore, the optimal ferrite width is 100 mm while the optimal ferrite-coil Z distance is 10 mm.

Based from the result in the last two columns of Table IV, the width of ferrite B is set to 100 mm and the ferrite-coil Z distance is set to 10 mm. Five different pairs of ferrite A,C width and ferrite-ferrite center distance are selected to validate the simulation result shown in Fig. 6. Table V displays the measured inductance matrix values and effective coil total resistances for the considered pairs. The comparison among P6, P7 and P8 indicates how the inductance matrix values and effective coil total resistances vary with ferrite A,C width when the ferrite-ferrite center distance remain constant. The comparison among P8, P9 and P10 indicates how the inductance matrix values vary with the ferrite-ferrite center distance when the ferrite A,C width remain constant. The measured values matches the simulated result

Table IV: Experimental measurement for ferrite B optimization

Pair	FW (mm)	FCZD (mm)	$M_{ab}(\mu H)$	$M_{ac}(\mu H)$	$M_{br}(\mu H)$	$R_b(mohm)$	$V_{dc}(V)$	$\eta_{coil}(\%)$
P1	50	0	-4.87	-9.03	11.57	342	172	88.27
P2	100	0	-5.06	-16.19	15.26	389	173	90.21
P3	150	0	-17.75	-39.77	18.45	441	392	91.83
P4	100	25	-4.61	-15.65	13.76	362	186	89.09
P5	100	10	-4.90	-16.42	14.63	336	178	90.68

FW: ferrite width, FCZD: ferrite-coil Z distance

Table V: Experimental measurement for ferrite A,C optimization

Pair	FW2 (mm)	FCD (mm)	$M_{ab}(\mu H)$	$M_{ac}(\mu H)$	$M_{ar}(\mu H)$	$R_a(mohm)$	$V_{dc}(V)$	$\eta_{coil}(\%)$
P6	100	175	-5.21	-19.51	10.69	162	542	91.27
P7	150	175	-12.80	-20.08	11.92	170	565	91.08
P8	200	175	-16.78	-24.56	13.05	175	616	93.29
P9	200	200	4.23	-16.78	12.76	174	382	93.01
P10	200	225	22.02	-15.64	13.09	177	456	92.94

FW2: ferrite A,C width, FCD: ferrite-ferrite center distance

displayed in Fig. 6 within an acceptable error. The last two columns of Table V display the estimated DC bus voltage and coil efficiency derived from the measured inductance matrix and effective coil total resistances in Table V. Among all the pairs P6-P10, only P9 is qualified due to its low DC bus voltage which is within the preferred solution range $V_{dc} \leq 400V$. Therefore, the optimal ferrite A,C width is 200 mm while the optimal ferrite-ferrite center distance is 200 mm.

Three-phase wireless system performance with optimized ferrite

In this section, the experimental measurements are completed for the ferrite pad with gap case and the optimized Y-axis ferrite bar with gap case under 1 kW output power, 300 V battery voltage and 85 kHz operating frequency. The ferrite pad with gap case is selected as benchmark to evaluate the performance of the optimized Y-axis ferrite bar with gap case regarding DC bus voltage and system efficiency. In particular, both the coil efficiency without power electronic losses and the DC-DC efficiency considering power electronic losses are measured to demonstrate the impact of ferrite placement towards power electronic losses. Fig. 7 shows the power electronic topology and the experiment setup for the three-phase wireless power transfer system.

Fig. 8 shows the waveform of the transmitter voltage and current of the three phase system using a full ferrite pad with gap at 5 cm receiver misalignment. Fig. 9 shows the waveform of the transmitter voltage and current of the three phase system using the optimized Y-axis ferrite bar with gap at 5 cm receiver misalignment. The yellow square voltage waveform in Fig. 8 and Fig. 9 is the voltage of phase B. By comparing the height of the yellow square voltage, it is obvious that the DC bus voltage required by the ferrite pad with gap case is higher than the optimized Y-axis ferrite bar with gap case. It is also important to notice that the optimized Y-axis ferrite bar with gap case can achieve soft switching while the ferrite bar with gap case is hard switching.

The required DC bus voltage for the 1 kW output power for the ferrite pad with gap case and optimized Y-axis ferrite bar with gap case are plotted in Fig. 10 left figure as a function of receiver misalignment. Due to the limitation of accessible DC bus voltage, the experiment validation is completed for receiver misalignment at 0 cm, 5 cm and 10 cm. The peak DC bus voltage difference is around 360 V at receiver 10 cm misalignment. The simulated, measured coil efficiencies and measured DC-DC efficiencies for the ferrite pad with gap case and optimized Y-axis ferrite bar with gap case are plotted in Fig. 10 right figure as a function of receiver misalignment. For coil efficiency, the ferrite pad with gap case is around 2.8% higher than the optimized Y-axis ferrite bar with gap case at 0 cm receiver misalignment since

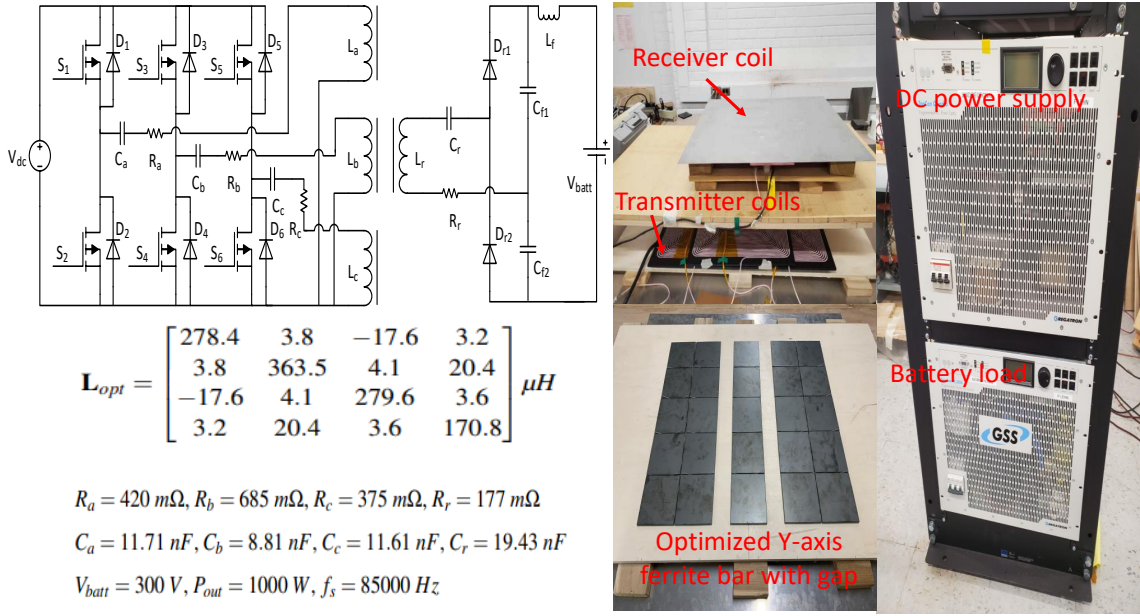


Fig. 7: Power electronic topology and experiment setup for the three-phase wireless system

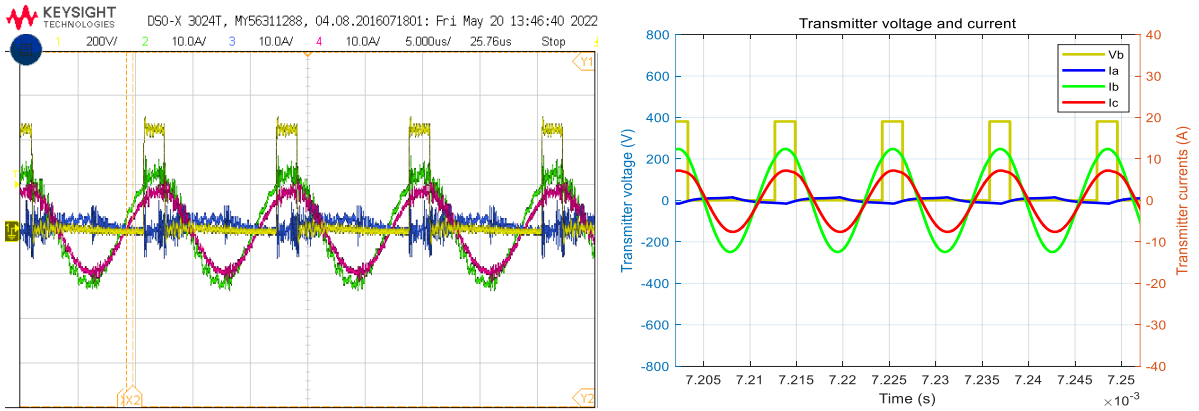


Fig. 8: Transmitter voltage and current for ferrite pad with gap at 5 cm receiver misalignment, oscilloscope measurement (left), simulation (right).

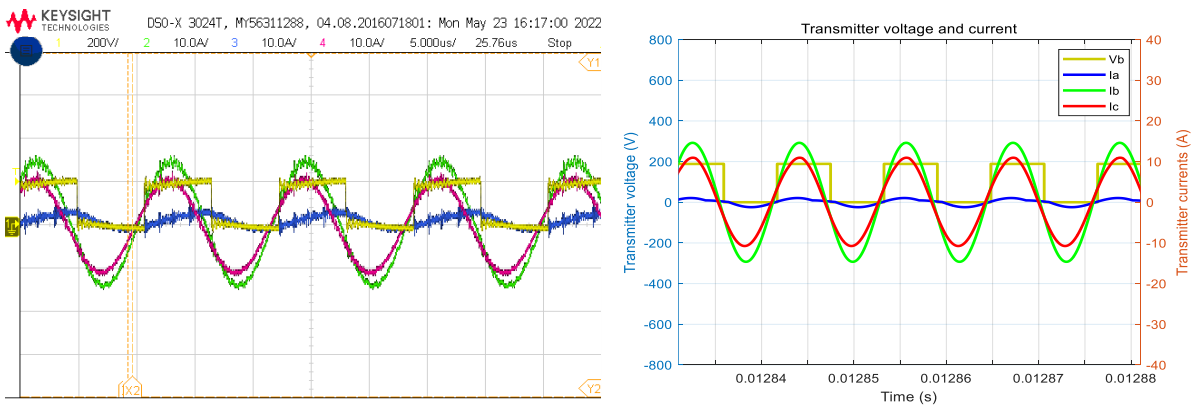


Fig. 9: Transmitter voltage and current for optimized Y-axis ferrite bar with gap at 5 cm receiver misalignment, oscilloscope measurement (left), simulation (right).

it has larger transmitter-receiver mutual inductances. However, if taking the power electronic loss into account, the DC-DC efficiency of the ferrite pad with gap case drops dramatically as receiver misaligned

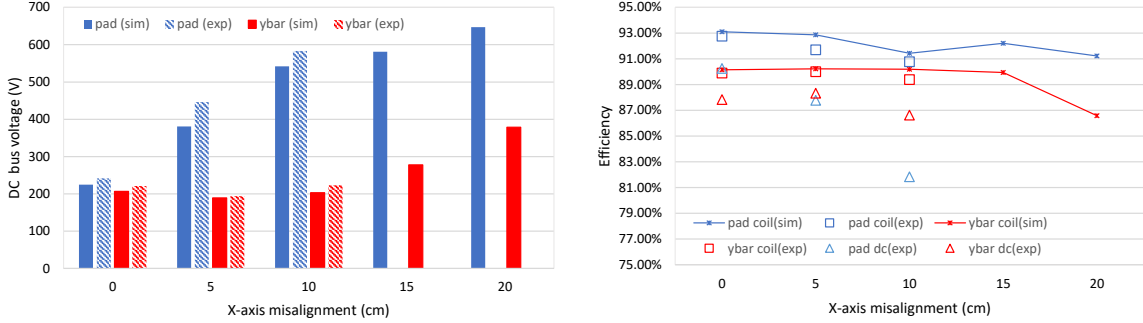


Fig. 10: Left figure: DC bus voltage for ferrite pad with gap and optimized Y-axis ferrite bar with gap at different receiver X-axis misalignment, right figure: efficiency for ferrite pad with gap and optimized Y-axis ferrite bar with gap at different receiver X-axis misalignment .

due to hard switching as shown in Fig. 8. The DC-DC efficiency of ferrite pad with gap case is around 4.8 % lower than the optimized Y-axis ferrite bar with gap case at 10 cm receiver misalignment.

Conclusion

This paper compares the ferrite placement in the aspects of orientation, size and position based on their impact to the inductance matrix. The proposed ferrite design reduces the ferrite usage by 40% but is capable of achieving higher DC-DC efficiency at receiver misalignment case and lowers the DC bus voltage by 62% at max.

References

- [1] H. Feng, R. Tavakoli, O. C. Onar and Z. Pantic, "Advances in High-Power Wireless Charging Systems: Overview and Design Considerations," in IEEE Transactions on Transportation Electrification, vol. 6, no. 3, pp. 886-919, Sept. 2020
- [2] M. Pathmanathan, S. Nie, N. Yakop and P. W. Lehn, "Field-Oriented Control of a Three-Phase Wireless Power Transfer System Transmitter," in IEEE Transactions on Transportation Electrification, vol. 5, no. 4, pp. 1015-1026, Dec. 2019
- [3] J. Pries, V. P. N. Galigekere, O. C. Onar and G. Su, "A 50-kW Three-Phase Wireless Power Transfer System Using Bipolar Windings and Series Resonant Networks for Rotating Magnetic Fields," in IEEE Transactions on Power Electronics, vol. 35, no. 5, pp. 4500-4517, May 2020
- [4] A. U. Ibrahim, W. Zhong and M. D. Xu, "A 50-kW Three-Channel Wireless Power Transfer System With Low Stray Magnetic Field," in IEEE Transactions on Power Electronics, vol. 36, no. 9, pp. 9941-9954, Sept. 2021
- [5] M. G. S. Pearce, G. A. Covic and J. T. Boys, "Reduced Ferrite Double D Pad for Roadway IPT Applications," in IEEE Transactions on Power Electronics, vol. 36, no. 5, pp. 5055-5068, May 2021
- [6] M. Mohammad, S. Choi, Z. Islam, S. Kwak and J. Baek, "Core Design and Optimization for Better Misalignment Tolerance and Higher Range of Wireless Charging of PHEV," in IEEE Transactions on Transportation Electrification, vol. 3, no. 2, pp. 445-453, June 2017
- [7] S. Nie, M. Pathmanathan, N. Yakop, Z. Luo, and P. W. Lehn, "Field orientation based three-coil decoupled wireless transmitter for electric vehicle charging with large lateral receiver misalignment tolerance," IET Power Electronics, vol. 14, no. 5, pp. 946-957.